

Generation of phonon quantum states and quantum correlations among single photon emitters in hexagonal boron nitride

Hugo Molinares¹, Fernanda Pinilla², Enrique Muñoz^{3,4}, Francisco Muñoz^{2,5}, Vitalie Eremeev^{6,7,*}

¹ Departamento de Ciencias Físicas, Universidad de La Frontera, Casilla 54-D, Temuco 4780000, Chile.

² Departamento de Física, Facultad de Ciencias, Universidad de Chile, Santiago, Chile.

³ Instituto de Física, Pontificia Universidad Católica de Chile, Santiago, Chile.

⁴ Center for Nanotechnology and Advanced Materials CIEN-UC, Avenida Vicuña Mackenna 4860, Santiago, Chile

⁵ Center for the Development of Nanoscience and Nanotechnology (CEDENNA), Santiago, Chile.

⁶ Instituto de Ciencias Básicas, Facultad de Ingeniería y Ciencias,

Universidad Diego Portales, Av. Ejército 441, Santiago, Chile and

⁷ Institute of Applied Physics, Academiei 5, MD-2028, Chișinău, Moldova.

(Dated: August 14, 2023)

Hexagonal boron nitride hosts one dimensional topologically-protected phonons at certain grain boundaries. Here we show that it is possible to use these phonons for the transmission of information. Particularly, (i) a color center (a single photon emitter) can be used to induce single-, two- and qubit-phonon states in the one dimensional channel, and (ii) two distant color centers can be coupled by the topological phonons transmitted along a line of defects that acts as a waveguide, thus exhibiting strong quantum correlations.

I. INTRODUCTION

Phonon-based quantum devices have attracted recent attention since, among other advantages over photons, phonons offer richer alternatives for coupling with several solid-state quantum systems[1–4]. There are proposals of systems comprising single photon emitters (SPEs), such as color centers in diamond, coupled by a one dimensional waveguide[5–7]. These reports show a promising way to entangle the SPEs. Also more exotic phenomena, such as phonon-phonon correlations[8] or phonon blockade[9–11] have been explored.

Recently, a two-dimensional system, hexagonal boron nitride (hBN), has attracted the attention as a material for quantum technologies due to the presence of SPEs covering the visible spectrum[12–16]. Despite the vast differences among these emitters, most of them share a common feature in their photoluminescence spectrum: well-separated and sharp phonon replicas, at $\sim 160 - 180$ meV[17, 18].

Additionally, hBN has been predicted to host one-dimensional topologically-protected phonons[19, 20] that do not experience dissipation and hence may preserve quantum correlations over comparatively long distances. Moreover, such phonon modes are immune to most types of disorder, as long as the relevant symmetry is protected (see Sec. II A). They seem ideal for playing the role of a phononic waveguide, able to keep coherence at long distances.

In this article we propose a system consisting of a layer of hBN hosting two SPEs coupled by a topologically protected phonon channel, see Fig. 1a. Our finding shows: (i) single-, two- and three-phonon Fock states along the phonon line, (ii) phonon-qubit state, and (iii)

quantum correlations between the SPEs. We will start in Sec. II by introducing the underlying physical system, its components and the effective Hamiltonian describing the interaction. Then, in Sec. III, we will show quantized single- and two-phonon states along the channel, induced by the SPEs and phonon-mediated correlations among the SPEs. Sec. IV summarizes our *ab initio* methods. Finally, we will mention our conclusions in Sec. V.

II. GENERALIZED MODEL

A. Topologically-protected phonon line in hBN

The unit cell of h-BN consists of two triangular sublattices formed by B and N atoms, respectively. At grain boundaries where the Z_2 symmetry is locally broken by the presence of a zig-zag edge of identical atomic species (see Fig. 1b), a topologically-protected phonon line (TPL) arises[19–21]. Breaking this lattice symmetry globally produces a well known gap-opening effect in the electronic spectrum of single-layer graphene[22, 23]. Here, the mechanism behind the emergence of the TPL seems analogous to the (electronic) valley Hall effect in bilayer graphene[24–28], which has been applied to other excitations in hexagonal lattices[29, 30]. This effect requires: (i) two *physically different* sublattices, in the sense that this difference has to open a band gap in the excitation spectrum, and (ii) the sublattices must be interchanged in some region. In the case of the valley Hall effect in bilayer graphene, a gate potential gives a different potential to both sublattices, opening a band gap, and a local inversion of the gate potential can interchange the sublattices, resulting in topological states at the regions where this inversion of voltage occurs. Similarly, in h-BN, the different masses of B and N atoms induces a band gap in the phonon spectrum (*i.e.* lifting a degeneracy at the K point). The remaining ingredient

* vitalie.eremeev@udp.cl

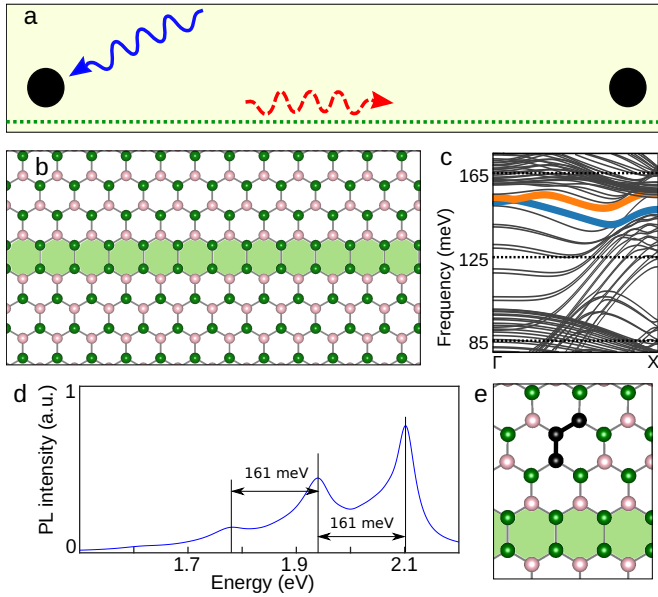


Figure 1. (a) Scheme of a grain boundary (green dashed line) coupling two SPEs (black circles) by means of a topologically-protected phonon mode (red curly arrow). Here, the SPEs can be excited by a laser (blue arrow). (b) Atomic representation of the grain boundary hosting the topologically protected phonons in h-BN, where each color represents a different atomic species. (c) Phonon subbands along the grain boundary, the topologically protected modes are highlighted by blue and orange. (d) Simulation of the photoluminescence spectra of a typical SPE in hBN (C₂C_N). (e) Model of a C₂C_N defect close to the grain boundary.

is switching both sublattices, which happens at certain grain boundaries (Fig. 1b). There are two types of these boundaries, B–B and N–N, in the figure only the B–B is shown, but the localized phonons of each boundary are similar. The phonon subbands of a cell with a pair of -well-separated- grain boundaries, B–B and N–N, are shown in Fig. 1c. The TPL have an energy centered at ~ 160 meV.

B. Single photon emitters in hBN

Most SPEs in h-BN are associated with substitutional carbon defects [31–34]. Depending on the atomic detail of the actual defects, the emission (zero-phonon line) can range from the near infrared to near ultraviolet energies[12, 18, 33]. Unlike color centers in diamond, the phononic sideband of the photoluminescence (PL) spectrum shows very prominent replicas with a shift of $\approx 160 - 180$ meV respect to the zero-phonon line[17, 18, 33]. They correspond to bond stretching modes, due to the different geometry of the ground and excited states of the SPEs, respectively. Fig. 1d shows a typical PL spectrum,[17, 33, 35] with a zero-phonon line at ≈ 2.1 eV. The energy of the phononic replicas is practically independent on the details of SPE[18]. There exist

a very different kind of SPEs in hBN which are based on vacancies, they have much softer and less defined phonon replicas in their PL spectrum[36, 37]. Along this article we will ignore these vacancy-related SPEs.

C. Coupling between the TPL and a SPE

The energy of the phonons resonating with the optical transition of a SPE is similar to that of the TPL. If the difference between both energies is small, the SPE's phonons could interact with the TPL, see Fig. 1e. If a second SPE is close to the TPL, both SPEs could be correlated by the TPL -which then plays the role of a waveguide- as depicted in Fig. 1a. Being dissipationless, the TPL can -in principle- link SPEs regardless of the distance among them, unlike typical phonons which are subject to umklapp scattering processes. Also, thanks to its inherent topological protection, this channel should be resistant to most types of scattering (*e.g.* lattice phonons), making it ideal for the transfer of information, even at high temperature. However, the TPL is not robust to disorder on the atomic masses (*i.e.* blurring the sublattice inversion), such as substitutional impurities, then a small coupling between both, SPEs and TPL can exist.

For a general picture of the proposed mechanism, a system of N SPEs interacting via a common -topologically-protected-phonon mode is considered in our theoretical model. To describe the TPL-mediated SPE-SPE interaction, we consider the common model of spin-boson interaction[38, 39], where the SPE plays the role of a local spin $\frac{1}{2}$ system (*i.e.* a two-levels system[40, 41]), with $|g\rangle = |\downarrow\rangle$ representing the ground state, and $|e\rangle = |\uparrow\rangle$ the excited state, respectively, in the SU(2) eigenbasis of $\hat{\sigma}^z$. Hence the whole ‘spin-phonon’ interacting system is governed by the following Hamiltonian (with $\hbar = 1$)

$$\hat{\mathcal{H}} = \hat{\mathcal{H}}_0 + \hat{\mathcal{H}}_I + \hat{\mathcal{H}}_P, \quad (1)$$

$$\hat{\mathcal{H}}_0 = \omega_M \hat{b}^\dagger \hat{b} + \sum_{j=1}^N \frac{\omega_j \hat{\sigma}_j^z}{2}, \quad (2)$$

$$\hat{\mathcal{H}}_I = \sum_{j=1}^N g_j \hat{\sigma}_j^z (\hat{b} + \hat{b}^\dagger), \quad (3)$$

$$\hat{\mathcal{H}}_P = \sum_{j=1}^N \Omega_j (\hat{\sigma}_j^+ e^{-i\omega_P t} + \hat{\sigma}_j^- e^{i\omega_P t}). \quad (4)$$

Here $\hat{\mathcal{H}}_0$ is the free Hamiltonian of the phonon and the SPEs, with energies ω_M and ω_j , respectively, and $\hat{\sigma}^z$ is the third Pauli matrix. $\hat{\mathcal{H}}_I$ is the interaction Hamiltonian and g_j is the spin-boson coupling strength (SPE-phonon in our system). Finally, $\hat{\mathcal{H}}_P$ represents an external pump provided by a laser of frequency ω_P , in order to drive coherently both SPEs. The ladder operators are denoted $\hat{\sigma}^+, \hat{\sigma}^-$. The spin-boson Hamiltonian has been the subject of extensive studies in the context

of strongly-correlated electronic systems, as an interesting scenario for the interplay between quantum criticality and entanglement. Former theoretical studies of this model[38–41] have been concerned about the coupling between a two-level system and a dissipative phonon thermal bath. In this case, an exact mapping to the anisotropic Kondo model allows to show numerically (via NRG)[39] and analytically (via Bethe-Ansatz)[38] that the corresponding spectral function of the phonon bath determines a crossover between an entangled regime and a disentangled one. In terms of this mapping, the corresponding Kondo temperature T_K that determines the transition is proportional to the strength of the “spin-flip operator”[38], a role that in our model is played by the external pump with magnitude Ω_j . We point out that, for some applications, it will not be necessary to consider the external pump, since the system will then evolve under the action of the Hamiltonian $\hat{\mathcal{H}}_0 + \hat{\mathcal{H}}_I$ and some dissipative mechanism. More details are given when discussing particular features. A derivation of the atomic Hamiltonian -excluding $\hat{\mathcal{H}}_P$ - is provided in the Appendix A.

Further, by applying the unitary transformation $\hat{U} = \sum_{j=1}^N \exp(i\omega_P \hat{\sigma}_j^z t)$ one gets the time-independent Hamiltonian

$$\begin{aligned} \hat{\mathcal{H}}' = & \omega_M \hat{b}^\dagger \hat{b} + \sum_{j=1}^N \frac{\Delta_j \hat{\sigma}_j^z}{2} + g_j \hat{\sigma}_j^z (\hat{b} + \hat{b}^\dagger) \\ & + \Omega_j (\hat{\sigma}_j^+ + \hat{\sigma}_j^-), \end{aligned} \quad (5)$$

with $\Delta_j = \omega_j - \omega_P$.

To have a reasonable estimate of the order of magnitude of the parameters ω_M and ω_j in $\hat{\mathcal{H}}'$, we performed density functional theory (DFT) calculations, in close agreement with other estimations reported in the literature[17, 19]. Estimating the coupling strength g_j from DFT is not straightforward and the details are presented in Sec. A of the Appendices.

D. Master Equation

To study the dynamics under realistic conditions, one should include the dissipation caused by the system-environment coupling. Consequently, we use the Markovian master equation (ME) for the system’s density matrix ($\hat{\rho}$) to simulate the time evolution under the dissipative and decoherent mechanisms acting on the SPEs and phonon subsystems, respectively. The generalized ME is defined as follows

$$\begin{aligned} \frac{d\hat{\rho}}{dt} = & -i[\hat{\mathcal{H}}', \hat{\rho}] + \frac{\gamma_b}{2} (1 + \bar{n}_b) \mathcal{L}[\hat{b}] + \frac{\gamma_b}{2} \bar{n}_b \mathcal{L}[\hat{b}^\dagger] \\ & + \sum_{j=1}^N \frac{\gamma_s}{2} (1 + \bar{n}_s) \mathcal{L}[\hat{\sigma}_j^-] + \frac{\gamma_s}{2} \bar{n}_s \mathcal{L}[\hat{\sigma}_j^+] + \frac{\gamma_\phi}{2} \mathcal{L}[\hat{\sigma}_j^z], \end{aligned} \quad (6)$$

where $\bar{n}_{b(s)}$ is the average number of quanta (*i.e.* thermal phonons) in the reservoir corresponding to the

phonon (SPEs) subsystem, respectively, and is calculated by the Bose-Einstein distribution as $\bar{n}_{b(s)} = (\exp[\hbar\omega_{b(s)}/(\kappa_B T)] - 1)^{-1}$. Initially each subsystem is in thermal equilibrium with its reservoir at a given temperature T , and κ_B is the Boltzmann’s constant here. In a general case, the dissipation and decoherence mechanisms are characterized by γ_b as the phonon damping rate, while γ_s and γ_ϕ are the “spin” (*i.e.* the local two-level system) rates for damping and pure dephasing, respectively. The Lindbladian superoperator is defined as $\mathcal{L}[\hat{O}] = 2\hat{O}\hat{\rho}\hat{O}^\dagger - \hat{O}^\dagger\hat{O}\hat{\rho} - \hat{\rho}\hat{O}^\dagger\hat{O}$.

E. System initialization

i) Initial phonon state. The phonon state is assumed to be initially in a thermal mixed state at temperature T , that in the coherent basis it can be written as

$$\hat{\rho}_b(0) = \frac{1}{\pi\bar{n}_b} \int |\xi\rangle\langle\xi| e^{-\frac{|\xi|^2}{\bar{n}_b}} d^2\xi, \quad (7)$$

where ξ in general is a complex number.

ii) Initial SPE state. Let us consider that each SPE is prepared in a superposition state like $|\psi_j(0)\rangle = \alpha_j|g\rangle + \beta_j|e\rangle$, with $|g\rangle = |\downarrow\rangle$ representing the ground state, and $|e\rangle = |\uparrow\rangle$ the excited state, respectively, in the $SU(2)$ eigenbasis of $\hat{\sigma}^z$. Here, $|\alpha_j|^2 + |\beta_j|^2 = 1$ and hence the density matrix for the subsystem of SPEs reads

$$\hat{\rho}_s(0) = \otimes_{j=1}^N |\psi_j(0)\rangle\langle\psi_j(0)|. \quad (8)$$

We point out that for $\alpha = \beta = 1/\sqrt{2}$ one has the particular case of a qubit state, which we will consider for some further calculations as an optimal condition to observe interesting effects to be discussed.

III. RESULTS

A. SPE-assisted generation of phonon quantum states

1. One SPE: Generation of phonon Fock states

The purpose of this work is twofold, the first goal is to analyze an adequate physical model that effectively describes the SPE-phonon interaction within a TPL approach, and the second goal is to apply this model for the engineering of phonon quantum states and quantum correlations between SPEs, these being important resources for current quantum technologies. An important tool for controlling and transferring quantum information, for example in phononic based interfaces, is related to the creation of quantum states such as Fock, qubits, and Schrödinger cats (superposition of coherent states) [15, 42–45]. In this context, in the following we propose such kind of quantum state engineering. Particularly we show in a dissipative evolution the possibility

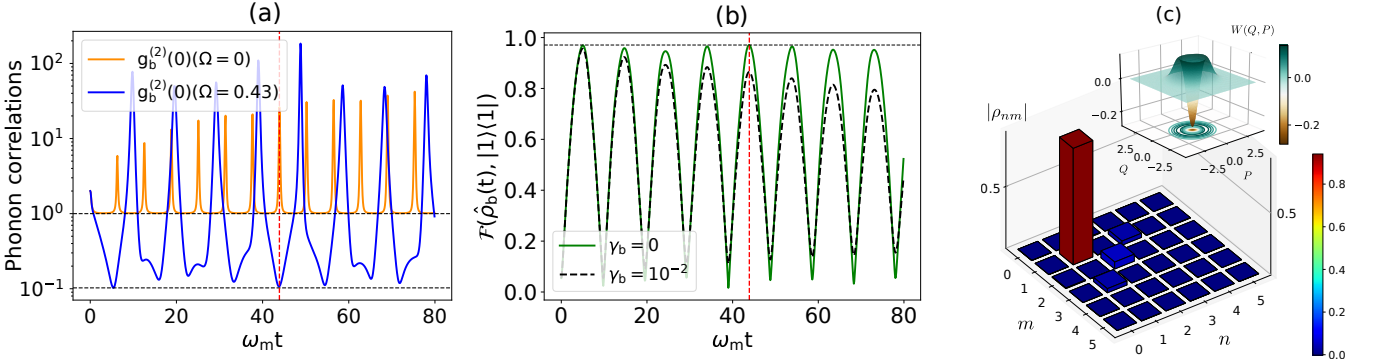


Figure 2. Generation of single-phonon Fock state with one SPE initially in a superposition state with $\alpha = \beta = 1/\sqrt{2}$ for $\Delta = 0$, $\Omega = 0.43$ and witnessed by: (a) Second-order correlation function, $g_b^{(2)}(0)$. (b) Fidelity of the Fock state $|1\rangle$ for different values of γ_b , i.e. TPL (green curve) and non-TPL (black curve). (c) Probability distribution in the basis of the Fock states at the dimensionless time $\omega_m t \approx 43.9$, corresponding to the maximal fidelity $\mathcal{F}_{|1\rangle} \sim 0.97$. (inset: Negative values of Wigner function witnesses a quantum state). Other parameters in units of ω_m are $g_1 = 0.33$, $\gamma_s = \gamma_\phi = 10^{-5}$ and $\bar{n}_b = 0.003$, $\bar{n}_s = 0$.

of preparation of Fock and qubit states for the phonon mode in the TPL and non-TPL regimes, considering the loss mechanisms for SPEs. We find that phonon quantum states can in principle be generated for any number of SPEs. However, since the total dissipation in this dynamics (see Eq. 6) is proportional to the number of SPEs, then the corresponding fidelity of the resulting quantum states decreases. Below we study the case of one SPE to fully analyze the observed effects, and in Appendix D we present the corresponding results for many SPEs.

Let us consider the simplest case, when there is only one SPE interacting with the TPL and this SPE is driven by a coherent pump field, as defined in Eq.(4). In that particular case, the ME becomes

$$\frac{d\hat{\rho}}{dt} = -i[\hat{\mathcal{H}}', \hat{\rho}] + \frac{\gamma_s}{2}\mathcal{L}[\hat{\sigma}^-] + \frac{\gamma_\phi}{2}\mathcal{L}[\hat{\sigma}^z], \quad (9)$$

where $\hat{\mathcal{H}}'$, as defined in Eq. 5, is considered for $N = 1$ SPE in this case. As the phonon is topologically protected from the interaction with the environmental thermal phonons, i.e. $\gamma_b = 0$, then the terms related to the phonon damping in Eq. 6 are absent here. Moreover, we emphasize that in our model the SPE energy corresponds to about 2 eV ≈ 483.6 THz, and hence the thermal environment at the room temperature gives $\bar{n}_s = 0$, thus the ME (Eq. 6) reduces to Eq. 9.

Now considering that there is one SPE initialized in a superposition state (Eq. 8) and driven by an external coherent source ($\hat{\mathcal{H}}_P$), while the phonons are initially in a thermal state (Eq. 7) with $\bar{n}_b = 0.003$. As a result of the SPE-TPL interaction and driving mechanism, Fock phonon states are generated at some intervals during the non-unitary dynamics, with the corresponding losses of the “spin” subsystem. To analyze the quantum statistics of the phonon dynamics, we numerically calculate the one-time second-order correlation function [46] for the

phonon mode

$$g_b^{(2)}(0) = \frac{\langle (\hat{b}^\dagger)^2 \hat{b}^2 \rangle}{\langle \hat{b}^\dagger \hat{b} \rangle^2} \quad (10)$$

ditionally, to witness the Fock state $|n\rangle$ we use complementary measures such as fidelity $\mathcal{F} = \sqrt{\langle n|\hat{\rho}_b|n\rangle}$ and the Wigner function. All these quantities are calculated in base of the reduced phonon state obtained as a partial trace on the “spin” subsystem of the global state by solving numerically [47] Eq. 9, i.e. $\hat{\rho}_b = \text{Tr}_s[\hat{\rho}]$.

Single-phonon Fock state.

The methodologies and setups for the preparation of individual phonon states [48–50] have attracted great interest in the last decade due to the many practical applications in quantum technologies. In the following we discuss the effect of the single-phonon Fock state within our proposal. In Fig. 2 we clearly see that, at some instants of dimensionless time, a phonon Fock state $|n = 1\rangle$ emerges. This effect is consistent with the following: (i) $g_b^{(2)}(0) < 0.5$ (see Fig. 2a); and (ii) the probability distribution on the Fock basis, and a negative value of the Wigner function (see Fig. 2c and inset). We solved the ME as a function of the parameters $\{\Omega, \Delta, \alpha\}$, and we found that the single-phonon Fock state is generated with the fidelity $\mathcal{F}_{|1\rangle} \sim 0.97$ at the dimensionless time $\omega_m t = 43.9$, and it is almost preserved in time for the case of the TPL, as shown by the green solid line in Fig. 2b. In contrast, in a regular phononic waveguide with losses (i.e. non-topologically protected) the fidelity of the Fock state decreases substantially in time, as shown by the black-dashed curve in Fig. 2b. This quantum effect for the TPL indicates that a coherently driven SPE, during its dynamics, exhibits time intervals when the generation of single phonon states at high fidelity is stimulated - a great practical application in many fields.

Fock states $|n = 2\rangle$ and $|n = 3\rangle$.

It is possible to prepare other Fock states, e.g. $|n = 2\rangle$

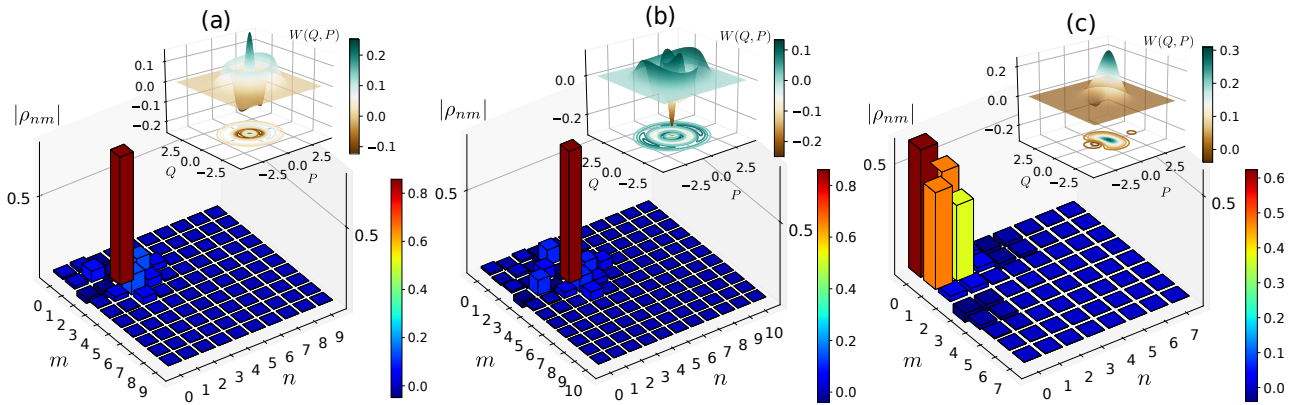


Figure 3. Dynamical preparation of the phonon Fock and Qubit states with one SPE: (a) Fock state $|n = 2\rangle$ prepared for $\alpha = 0.30$, $\Omega = 0.63$ and $\Delta = 1.23$. The maximal fidelity $\mathcal{F}_{|2\rangle} = 0.92$ is observed at $\omega_{mt} = 146.5$. (b) Fock state $|n = 3\rangle$ prepared for $\alpha = 0.55$, $\Omega = 1.30$ and $\Delta = 0.60$, with the maximal fidelity $\mathcal{F}_{|3\rangle} = 0.92$ occurring at $\omega_{mt} = 344.6$. (c) Phonon Qubit state $(|0\rangle + |1\rangle)/\sqrt{2}$ with maximal fidelity $\mathcal{F}_{\text{qubit}} = 0.98$ at $\omega_{mt} = 66.2$ for $\alpha = 1$, $\Omega = 0.27$ and $\Delta = 1.87$. Other parameters are the same as in Fig. 2.

and $|n = 3\rangle$, by appropriately tuning the parameters Ω , Δ and α . For instance, the Fock state $|2\rangle$ is optimally prepared for the combination of parameters presented in Fig. 3a. This effect can be witnessed by the correlation function $g_b^{(2)}(0) \rightarrow 0.5$ (not presented here), and further corroborated by the probability distribution in the Fock basis, as well as by the negative value of the Wigner function, thus indicating the quantum state, see inset in Fig. 3a. The fidelity of this state reaches $\mathcal{F}_{|2\rangle} \sim 0.92$. On the other hand, the Fock state $|n = 3\rangle$ can be prepared in a similar way, see Fig. 3b. For the sake of space, do not show explicitly the figures containing the dynamics of the second order correlation function and the fidelities for the Fock states considered here, however these quantities were also analyzed and display similar results as the ones shown in Figs. 2a-b. Based on these results, the information of the time instants corresponding to the maximum values of the fidelities is obtained and indicated in Fig. 3.

2. One SPE: Generation of the phonon Qubit state

Since the phonon Fock states are realizable in our proposal, one can expect to prepare a phonon qubit, which is in fact a superposition of the Fock states $|0\rangle$ and $|1\rangle$. A phonon qubit state can serve as a key element in a solid-state quantum network, thus representing a candidate to replace its “cousin”, the photonic qubit, used in photon-based setups [51]. Methodologies for preparing phonon qubit states nowadays are limited to very few types of interfaces, particularly based on micromechanical resonators [43, 52, 53]. Here, we show that a high-fidelity phonon qubit, $(|0\rangle + |1\rangle)/\sqrt{2}$, could be prepared in our proposal using the TPL configuration. In Fig. 3c one sees clearly how the qubit state is witnessed by the probability distribution in the Fock basis and the negative part of the Wigner function (see inset).

B. Phonon-assisted SPE-SPE Quantum Correlations

1. Generation of Entanglement

In this subsection and the next one, we are interested in studying the quantum correlations established in time between two distant SPEs that interact with a common phononic mode, be it TPL or non-TPL. The correlations will be measured using the Concurrence (Entanglement) and Quantum Discord quantifiers. In addition to the analytical and numerical calculations, we compare these theoretical results with those obtained from experimentally emulated measurements (see Sec. III C) of these correlations performed in the IBM Quantum [54] simulator. Our excellent agreement between the theoretical and quasi-experimental results may open new avenues for the applications of quantum information protocols to condensed matter systems, where experimental investigations are still complex and expensive to carry out.

Let’s consider two SPEs initialized in the state defined by Eq. 8, and as compared to the previous protocol of generation of phonon Fock states, here is not necessary to include a driving field, *i.e.* $\Omega = 0$ in Eq. 5. On the one hand, we take into account the decoherence mechanisms for SPEs such as damping and dephasing and, on the other hand, the TPL is protected from decoherence. In order to compare with a non-topologically protected phonon mode, we calculate the quantum correlations considering the phonon damping rate $\gamma_b \neq 0$ within the bath at the temperature T . Therefore, the ME (Eq. 6) will be numerically solved for these two configurations.

The quantum correlations witnessed here as Entanglement for a system of two qubits (SPEs) can be quantified by the Concurrence (\mathcal{C}) [55]. We resume here the conceptual calculation of the Concurrence. For a general mixed state $\hat{\rho}_{AB}$ of two qubits, one defines $\tilde{\rho}$ to be the “spin”-

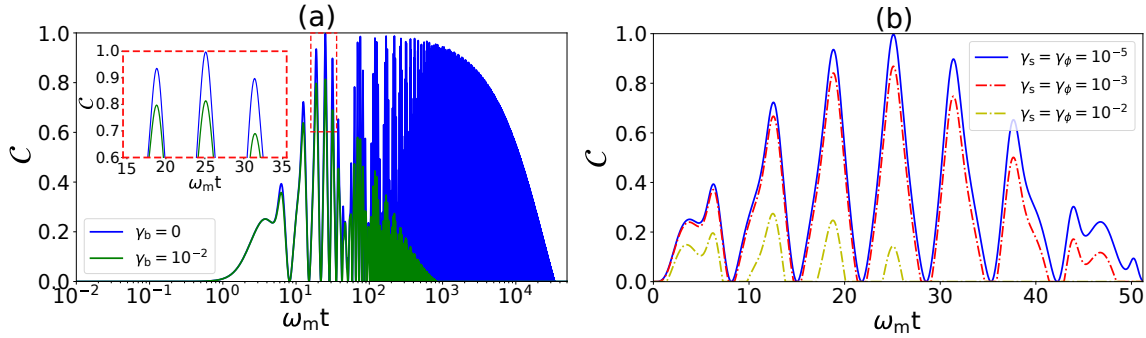


Figure 4. Dynamics of Concurrence (\mathcal{C}) for two SPEs initially in a superposition state (Eq. 8) with $\alpha = \beta = 1/\sqrt{2}$. (a) Concurrence for TPL (blue) and non-topological phonon (green) calculated for SPE losses as $\gamma_s = \gamma_\phi = 10^{-5}$; (inset: zooming of a MES for TPL). (b) Concurrence at early stage for TPL and varying the SPE losses. Other parameters in units of ω_m are: $g_1 = g_2 = 0.33$, $\Omega = 0$, $\bar{n}_b = 0.003$, $\bar{n}_s = 0$.

flipped state $\tilde{\rho}_{AB} = (\hat{\sigma}^y \otimes \hat{\sigma}^y) \hat{\rho}_{AB}^* (\hat{\sigma}^y \otimes \hat{\sigma}^y)$, where $\hat{\rho}^*$ is the complex conjugate of $\hat{\rho}$, and $\hat{\sigma}^y$ is the Pauli operator. Therefore, the Concurrence is defined as

$$\mathcal{C}(\rho) = \max\{0, \lambda_1 - \lambda_2 - \lambda_3 - \lambda_4\}, \quad (11)$$

where $\{\lambda_i\}$ are the square roots in decreasing order of the eigenvalues of the non-hermitian matrix $\hat{\rho}\hat{\rho}^*$. To point out here, the Concurrence normalized to one witnesses an entangled two-qubit state $\hat{\rho}_{AB}$ by obeying the condition $0 < \mathcal{C} \leq 1$. Hence, one has a maximally entangled state (MES) when $\mathcal{C} = 1$, and for $\mathcal{C} = 0$ there is no entanglement at all, so the two-qubit state can be written as a product of separated states, i.e. $\hat{\rho}_{AB} = \sum p_i \hat{\rho}_i^A \otimes \hat{\rho}_i^B$. Famous examples of MES are the well-known four Bell states [56], however, it is possible to have another types of MES, which are not necessarily Bell states.

In the following, we study the evolution of the Entanglement between the two SPEs. For example, in Fig. 4a, extensive time dynamics of Entanglement (\mathcal{C}) are shown for the TPL (blue curve) and for phonon damping (green curve) models. Both correlations are promptly generated, and at an early stage exhibiting a MES ($\mathcal{C} \sim 1$) for the topologically protected configuration, see the inset in Fig. 4a (blue curve). The MES is very useful for quantum information applications [56–58]. However, the quantum correlations decrease exponentially under the dissipation mechanisms of the SPEs and are totally lost at long times. The quantitative effect of such dissipation on the Entanglement is shown in Fig. 4b. One sees that the Entanglement is a very fragile quantum resource that can be quickly destroyed by strong dissipation, however it is possible to engineer some protection protocols like the one proposed here, via topological phonon state, and one intuitively expects that such protocol will be more efficient for a stronger spin-phonon interaction. An important remark is that in our model the distance between the SPEs can be arbitrarily large without compromising the coherence. In general, there are two mechanisms of decoherence related with distances:

- In electronic systems such as the SPEs, the inter-

actions responsible for the coherence decrease exponentially with distance (e.g. a direct SPE-SPE interaction should suffer from this).

- The number of particles to interact with increases with distance, thus increasing the phonon damping. In one-dimension, the damping should increase geometrically (e.g. a non-topologically protected phonon line should be affected).

As a main result of this subsection, we show in Fig. 4 the generation of SPE-SPE quantum Entanglement (inseparable bipartite state) only stimulated by the phonon-mediated interaction, since in this protocol there is no external driving of SPEs, in contrast to the protocol of phonon Fock state generation (sec. III A).

2. Quantum Discord: Generation and freezing effects

The quantum correlations beyond the Entanglement can be witnessed by another quantity known as Quantum Discord (\mathcal{QD}) [59–61], and sometimes it is used as an alternative quantum resource in quantum information technologies [62–65]. The main feature of \mathcal{QD} is to quantify the quantum correlations for the separated states, i.e. those not entangled, and to discriminate which of these states contains quantum (not limited to entanglement) or pure classical correlations. For a pedagogical overview of the concepts and definitions related to \mathcal{QD} , we recommend a mini-review [66], and for more comprehensive material the review [67]. On the other hand, we point out that the analytical calculation of the \mathcal{QD} is not a straightforward calculation, but it is generally considered a difficult mathematical problem because it involves a minimization (maximization) procedure over many parameters. However, there are few particular cases for which the \mathcal{QD} can be calculated relatively easily, one of this is the case of the Bell-diagonal (BD) states [56, 61, 68]. In the $SU(2)$ basis of the Pauli matrices $\hat{\sigma}^i$ ($i = \{1, 2, 3\} \equiv \{x, y, z\}$), defined by an X-type density

matrix in Bloch form, the BD state for the system of two SPEs is

$$\hat{\rho}_{BD}(0) = \frac{1}{4} \left(\hat{\mathbb{1}}_2 \otimes \hat{\mathbb{1}}_2 + \sum_{i=1}^3 c_i \hat{\sigma}^i \otimes \hat{\sigma}^i \right), \quad (12)$$

where c_i are real constants satisfying the constraints $-1 \leq c_i \leq 1$, such that $\hat{\rho}$ is a well defined density operator; $\hat{\mathbb{1}}_2$ is the identity operator. Since in the initial state the SPEs and phonon are disentangled (no previous interaction), the density matrix of the whole system can be written as a tensor product between the subsystems:

$$\hat{\rho}(0) = \hat{\rho}_{BD}(0) \otimes \hat{\rho}_b(0), \quad (13)$$

where $\hat{\rho}_b(0)$ is the initial phonon state defined in Eq. 7.

The first situation we would like to discuss here is when two SPEs are initially prepared in a BD state without Entanglement, *i.e.* with $\mathcal{C} = 0$. Before the concept of \mathcal{QD} [59, 60] was introduced, the disentangled (separable) states were considered to exhibit only classical correlations. However, some disentangled states can evidence quantum correlations witnessed by the \mathcal{QD} , e.g. see the case of Werner state in [61]. In order to observe the dynamics of such states in our model for the TPL regime, let us consider the case of initial SPEs prepared in a state with only classical correlations, a particular BD state for $\{c_i\} = \{1, 0, 0\}$, *i.e.* in this case $\hat{\rho}_{BD}(0) = \frac{1}{4} (\hat{\mathbb{1}}_2 \otimes \hat{\mathbb{1}}_2 + \hat{\sigma}^x \otimes \hat{\sigma}^x)$. For this state, it is straightforward to check that $\mathcal{C} = 0$, $\mathcal{QD} = 0$ and the classical correlation is equal to one. It is interesting to discover that under non-dissipative or dissipative dynamics, the spin-boson model considered in our proposal of SPEs-phonon interaction, will exhibit the emergence of \mathcal{QD} , however the entanglement is never generated, *i.e.* $\mathcal{C} = 0$ throughout the whole dynamics. In Fig. 5 we present the non-dissipative dynamics of the \mathcal{QD} calculated analytically (using Eq.B2) for various values of the SPE-phonon coupling. It is observed that \mathcal{QD} is not created for the case of $g = 0$ (without SPE-phonon interaction) and as the SPE-phonon interaction increases, \mathcal{QD} is created. In addition, a critical value is observed for the SPE-phonon interaction, where \mathcal{QD} will not increase more but will remain constant for a given period of time. Such particular effect looks similar to the one called “Quantum Discord Freezing” (QDF) [67]. In Fig. 5, one sees that for $g/\omega_m = 0.33$ (a value that resulted in our microscopic calculation) QDF is not observed, but for $g/\omega_m = 0.60$ it is well manifested (see the green curve), and for a higher value of the SPE-phonon strength, the QDF begins to be partially destroyed (see the magenta curve). This effect can be related to the condition of the strong-coupling limit for the spin-boson model [69]. We note here that the dissipative dynamics for the same BD state preserves \mathcal{QD} generation and QDF effects, the only difference from lossless dynamics is that \mathcal{QD} will evidence an exponential decay and will vanish at long times, an

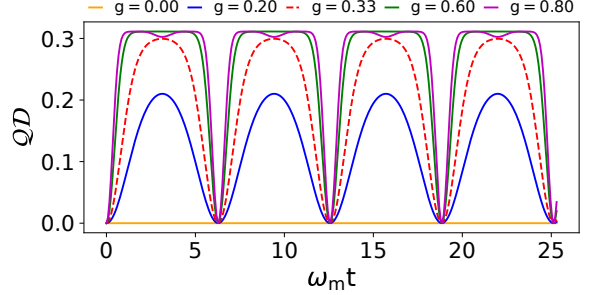


Figure 5. Lossless dynamics of Quantum Discord (\mathcal{QD}) for two SPEs initialized in a BD state with $c_1 = 1$, $c_2 = c_3 = 0$. Here the spin-phonon coupling $g_1 = g_2 = g$, $\Omega = 0$, and $\bar{n}_b = 0.003$.

unavoidable condition for quantum correlations in a dissipative system.

Now, let us study the dissipative evolution for another initial BD state, which exhibits commonly known QDF effects, similar to those studied in [70–73] and other works. In order to analyze such a “freezing” effect for \mathcal{QD} , we consider the initial BD state with $\{c_i\} = \{1, -0.9, 0.9\}$, which has a non-zero Entanglement (\mathcal{QD}) and non-zero \mathcal{QD} . For this quantum protocol, we propose to study three different situations: *i*) Unitary dynamics (no losses at all); *ii*) Dynamics for TPL with losses of SPEs; *iii*) Dynamics for non-topological phonon ($\gamma_b = 10^{-2}$) with losses of SPEs. The losses of SPEs are defined by $\gamma_s = \gamma_\phi = 10^{-5}$ for a numerical calculation of Eq. 6. In addition to the dynamics of \mathcal{QD} , we compute the Concurrence for the same situations. The unitary dynamics of \mathcal{QD} is calculated analytically as explained in Appendix B, whilst the dissipative dynamics can be computed numerically by solving the general ME, Eq. 6.

As a result, in Fig. 6 the evolution of the initial two-qubit BD state exhibits an interesting effect, since the \mathcal{QD} is frozen periodically in time (plateaux regions). In contrast, the Concurrence does not evidence such effect, only exhibiting the so-called “Entanglement Sudden Death” effect (the regions where $\mathcal{C} = 0$). In Fig. 6a we compare the numerical and analytical (Eq. B2) results, that fit together perfectly for the unitary dynamics of the full system. When the thermal losses are included into the dynamics, the effect of freezing is destructively affected in time, as observed in Fig. 6(b-c). However, for the case of TPL as compared to the non-TPL case, the freezing is protected for a longer time period, as seen by comparing Figs. 6b and 6c.

As the main conclusion of this subsection, we point out that the \mathcal{QD} can be generated and the QDF observed for a particular type of BD states, in which the qubits (SPEs here) are initialized, and for a certain range of values of the model parameters, such as the relationship between coupling and decoherence rates within the subsystems.

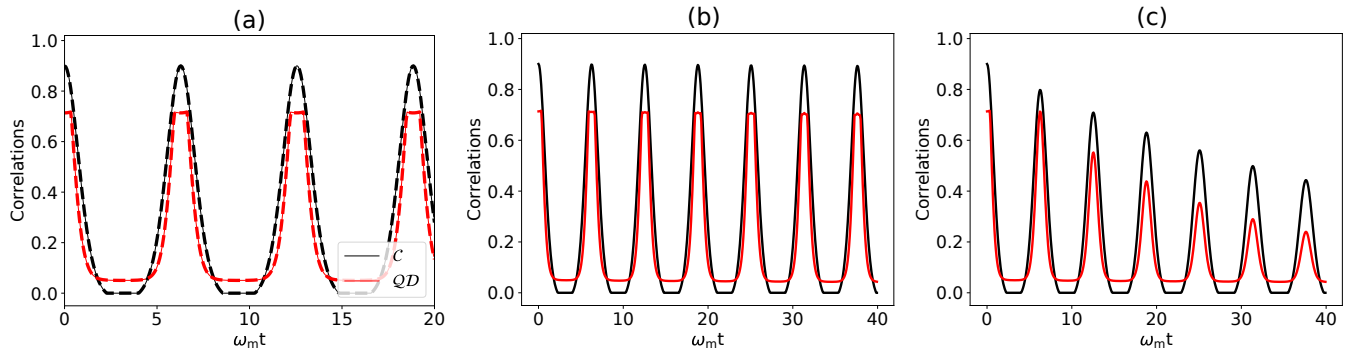


Figure 6. Dynamics of Quantum Discord (QD) and Concurrence (C) for SPEs initialized in a BD state (12). (a) Lossless dynamics considering the numerical simulation of Eq. (6) (solid line), and analytical solution in Eq. (B2) (dashed line). (b) Dynamics in case of TPL ($\gamma_b = 0$) with losses for SPEs as $\gamma_s = \gamma_\phi = 10^{-5}$. (c) Dynamics in case of non-topological phonon ($\gamma_b = 10^{-2}$) with the losses for SPEs as in (b). Other parameters are the same as in Fig. 4 with additional ones: $c_1 = 1$, $c_2 = -0.9$, $c_3 = 0.9$.

C. Experimental simulation of the Quantum Correlations

In the following, we propose to simulate an experimental measurement of the evolution of the quantum correlations in case of the SPEs initialized in the Bell-diagonal state as in Eq. 12. For this purpose, we use the IBM Qiskit simulator [54], where the intrinsic quantum noise is taken into account during the calculation, thus simulating a quasi-realistic quantum measurement. This quantum experiment is emulated via a quantum circuit, which is presented in details in the Appendix C.

Solving the Lindblad ME, see Eq. 6, on a classical computer and on the IBM’s quantum simulator, the quantum correlations are shown in Fig. 7. The solid lines represent the solution of the master equation on a classical computer, and the dots represent the result from the quantum simulator. A very good correspondence is found between the theoretical and quasi-experimental results, thus demonstrating the possibilities of existing quantum simulators and processors such as IBM, to be successfully used to emulate results similar to the experimental ones

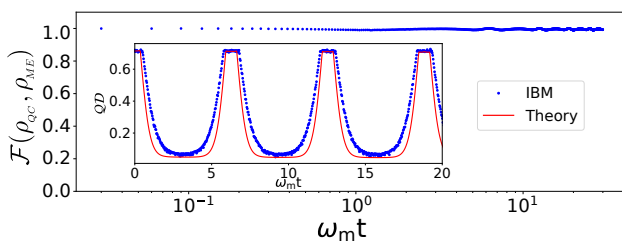


Figure 7. Fidelity of the quantum states calculated on quantum simulator and on a common computer. Inset: Quantum Discord (QD) for two SPEs initialized in a Bell-diagonal state (Eq. 12). The solid lines are the solutions on a classical device (common computer), the dots are generated using the IBM Quantum Qiskit simulator. The parameters here are the same as in Fig. 6(b), *i.e.* for TPL ($\gamma_b = 0$).

in problems like the one proposed in this work.

IV. METHODS

The electronic structure calculations were made with density functional theory, implemented by the VASP code[74–76]. We used a cutoff of 500 eV, PAW[77] pseudopotentials and the Perdew-Burke-Ernzerhof description of the exchange-correlation[78]. A single k-point (Γ) was used in the supercell calculation. Pyprocar[79] was used for the analysis of the electronic structure, and Phonopy[80] for the calculation of phonons. The photoluminescence spectra was calculated by following Ref [81]. Some preliminary calculations were made with density functional tight-binding[82, 83]. For the numerical solving of the master equations and calculations of the quantum states and correlations we use the Quantum Toolbox in Python - "QuTiP" [47]. The quantum circuit was emulated on the IBM Qiskit simulator [54].

V. CONCLUSIONS

The two-dimensional material hexagonal boron nitride has two types of defects with great potential for quantum applications: single photon emitters (SPEs) and topologically protected phonon lines (TPL). As described in this work, while the first are localized defects, the second represent a line of atomic defects (*e.g.* a grain boundary). Interestingly, the typical phonon frequencies of both are similar, resulting in a sizable interaction among them. This allows the use of the TPL as a topologically protected one-dimensional waveguide, connecting two SPEs within a single layer of hexagonal boron nitride, that preserves quantum correlations (characterized by Entanglement and Quantum Discord) for comparatively long periods of time.

This proposal shed light on the properties of this phononic quantum device. We showed that in a dissipative system -upon laser pumping- one SPE can excite a single as well as larger Fock states (*e.g.* $|n = 2\rangle$ and $|n = 3\rangle$) of the TPL. In addition to the Fock states, we show the possibility for creation of a phonon qubit state with a high fidelity, $\mathcal{F} \sim 0.98$. The quantum states were corroborated by measuring the second-order correlation functions ($g^{(2)}$), fidelities and the Wigner functions. When two SPEs interact with the TPL -plus the pumping field- the Fock and qubit states can also be excited, but at lower fidelities because the global losses increase. In this way, two SPEs can interact via the TPL by exchanging phonons. Both SPEs are entangled for several cycles of the evolution, as measured by the quantum concurrence. The coherence is practically independent of the separation between both SPEs, thanks to the topological protection against scattering provided by the TPL.

In summary, our theoretical results suggest that arrays of SPEs connected by TPL phononic waveguides represent promising candidates for quantum information applications.

ACKNOWLEDGMENTS

This research was funded by FONDECYT through grants 1231487, 1220715, and 1230440; by the Center for the Development of Nanosciences and Nanotechnology, CEDENNA AFB 220001; Conicyt PIA/Anillo ACT192023. Powered@NLHPC: This research was partially supported by the supercomputing infrastructure of the NLHPC (ECM-02).

Appendix A: Derivation of the microscopic Hamiltonian

Let's consider a SPE with only two states involved in the transition. The energy depends parametrically on the nuclear coordinates:

$$H(\mathbf{R}) = \sum_{i=1}^2 E(\mathbf{R}) c_i^\dagger c_i, \quad (\text{A1})$$

where E refers to the energy of each level, and c_i is a fermionic annihilation operator.

The minimum energy geometry for the ground- and excited-levels will differ. We will denote $\mathbf{R}^{(g)}$ and $\mathbf{R}^{(e)}$ as the *relaxed* positions of the ground and excited states. Taking the coordinates of the ground state as reference ($\mathbf{R}^{(g)}$), and expanding to the first order:

$$H(\mathbf{R}^{(e)}) = \sum_{i=1}^2 E(\mathbf{R}^{(g)}) c_i^\dagger c_i + \sum_{i=1}^2 \sum_{j=1}^{3N} \nabla_j E_i(\mathbf{R}^{(g)}) \Delta \mathbf{R}_j c_i^\dagger c_i, \quad (\text{A2})$$

with $\Delta \mathbf{R} = \mathbf{R}^{(e)} - \mathbf{R}^{(g)}$.

By using $\Delta \mathbf{R} = a^\dagger + a$ (with a, a^\dagger bosonic operators), the last term takes the form of a typical electron-phonon interaction:

$$H_{eph} = \sum_{i=1}^2 \sum_{j=1}^{3N} \mathbf{F}_{i,j} \Delta \mathbf{R}_j c_i^\dagger c_i = \sum_{i=1}^2 \sum_{j=1}^{3N} g_{i,j} (a_j^\dagger + a_j) c_i^\dagger c_i \quad (\text{A3})$$

where the electron-phonon coupling strength is $g_{i,j} = \mathbf{F}_{i,j} = \nabla_j E_i(\mathbf{R}^{(g)})$.

It is useful to switch to the basis of the phonons of the systems:

$$\mathbf{F}_{i,k} = \sum_{j=1}^{3N} \mathbf{F}_{i,j} \Delta \mathbf{r}_{k,j} \quad (\text{A4})$$

$$\Delta \mathbf{R}_k = \sum_{j=1}^{3N} \Delta \mathbf{R}_j \Delta \mathbf{r}_{k,j} \quad (\text{A5})$$

with $\Delta \mathbf{r}_{k,j}$ the j coordinate of k -th (normalized) phonon mode. In this basis the interaction Hamiltonian is:

$$H_{eph} = \sum_{i=1}^2 \sum_{k=1}^{3N} g_{i,k} (b_k^\dagger + b_k) c_i^\dagger c_i, \quad (\text{A6})$$

with b_k, b_k^\dagger bosonic operators acting on the phonon modes. In the main article we are interested only in the phonon mode belonging to the TPL (*i.e.* only a single term $k = k_0$ is relevant for our model).

The relevant parameters are: (*i*) the zero-phonon line (*i.e.* the energy of the single photons), this value can be obtained from the literature[12, 17], and it ranges from the near-infrared and the near-UV. We used a typical value of 2.1 eV. (*ii*) The energy of the (topological) phonons localized at the grain boundary, ~ 150 meV. And (*iii*) the coupling between the topological phonons and the (vibronic) optical transition. This strength can be calculated from the atomic forces on the ground state after a optical excitation, by expanding the atomic displacements in the basis of the phonons, see Eq. A4, only the component of $\mathbf{F}_{i,k}$ with index k representing the topological phonon needs to be selected. We calculated a strength of ~ 0.02 eV/Å between the optical transition and the topological phonon line. To get a coupling strength $g_{i,k}$ in units of eV, we will scale it by the lattice parameter of hBN, $a \approx 2.5$ Å.

Appendix B: Analytical calculation of the density matrix for the BD states

For the lossless case it is possible to get the analytical dynamics of BD. Therefore, considering the Hamiltonian in the interaction picture, Eq. 5 without the driving term (*i.e.* $\Omega = 0$) one has

$$\hat{\mathcal{H}}_{int} = \hat{b}^\dagger \hat{b} + \sum_{j=1}^2 \frac{\omega_0 \hat{\sigma}_j^z}{2} + g_0 \hat{\sigma}_j^z (\hat{b} + \hat{b}^\dagger). \quad (\text{B1})$$

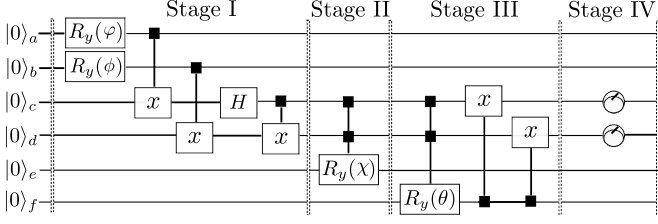


Figure 8. Quantum circuit simulating the dissipative evolution of the two SPEs interacting with TPL under the losses mechanisms of the SPEs. This circuit emulates the quantum evolution of the whole system equivalent to the master equation 6.

Then the unitary evolution operator reads

$$\begin{aligned}\hat{U}(t) &= \exp[-it\hat{H}_{int}] \\ &= \exp[g_0(\hat{\sigma}_1^z + \hat{\sigma}_2^z)(\eta\hat{b}^\dagger - \eta^*\hat{b})] \exp[-i\hat{b}^\dagger\hat{b}t],\end{aligned}$$

where $\eta = 1 - e^{-it}$. In Eq. B1 we have normalized the parameters by ω_m , i.e. $g_0 = g_j/\omega_m$ and $\omega_0 = \omega_j/\omega_m$.

The dynamics of the state of two SPEs is given by the density operator $\hat{\rho}_{s_1, s_2}(t) = Tr_b\{\hat{U}(t)(\hat{\rho}_{BD}(0) \otimes \hat{\rho}_b(0))\hat{U}^\dagger(t)\}$.

After a straightforward calculation, one obtains the two-qubit state in a X -form

$$\hat{\rho}_{s_1, s_2}(t) = \frac{1}{4} \begin{pmatrix} 1 + c_3 & 0 & 0 & (c_1 - c_2) \cdot A \\ 0 & 1 - c_3 & c_1 + c_2 & 0 \\ 0 & c_1 + c_2 & 1 - c_3 & 0 \\ (c_1 - c_2) \cdot A & 0 & 0 & 1 + c_3 \end{pmatrix} \quad (B2)$$

where $A = Tr_b\{D(4g_0)e^{-i\hat{b}^\dagger\hat{b}t}\hat{\rho}_b(0)e^{i\hat{b}^\dagger\hat{b}t}\}$, with $D(4g_0) = e^{4g_0(\eta\hat{b}^\dagger - \eta^*\hat{b})}$. Since we are studying unitary dynamics here, then the density matrix in Eq. B2 retains its X -form during evolution and the QD can be calculated analytically based on the detailed explication in Ref. [68] (see Eqs. 23-26 therein), where the off-diagonal marginal elements in Eq. B2 become time dependent in our case, according to the time function of A defined above.

Appendix C: Quantum circuit for the IBM Quantum Simulator

In order to realize a quantum experiment on IBM Qiskit simulator one needs to emulate evolution of the system and measurement of the interested quantities via a quantum circuit running on the simulator. Therefore, in Fig. 8 we show the quantum circuit that simulates the open dynamics of the two dissipative SPEs interacting via TPL and governed by the master equation Eq. 6.

The quantum circuit involves several operational stages as can be observed in Fig. 8. Following Refs. [84, 85], it is possible to prepare the SPEs in Bell diagonal states (see *stage I*). Here, the single-qubit rotation

about the Y axis, $R_y(\varphi)$ and $R_y(\phi)$, are applied on the lines $|0\rangle_a$ and $|0\rangle_b$, respectively. The single-qubit rotation about the Y axis is generally defined for an angle ϑ as:

$$R_y(\vartheta) = e^{-i\frac{\vartheta}{2}\hat{\sigma}^y} = \begin{pmatrix} \cos(\vartheta/2) & -\sin(\vartheta/2) \\ \sin(\vartheta/2) & \cos(\vartheta/2) \end{pmatrix}. \quad (C1)$$

The aforementioned phases, φ and ϕ can be obtained using the expressions [84, 85]:

$$\varphi = 2 \arccos \sqrt{p_{00} + p_{01}}, \quad (C2)$$

$$\phi = 2 \arccos \sqrt{p_{00} + p_{10}}. \quad (C3)$$

Here $p_{00}, p_{01}, p_{10}, p_{11}$ are the parameterization between Pauli and Bell basis $\{p_{jk}\}_{j,k=(0,1)} \rightarrow (c_1, c_2, c_3)$ given by

$$p_{00} = \frac{1 + c_1 - c_2 + c_3}{4}, \quad (C4)$$

$$p_{01} = \frac{1 - c_1 + c_2 + c_3}{4}, \quad (C5)$$

$$p_{10} = \frac{1 + c_1 + c_2 - c_3}{4}, \quad (C6)$$

$$p_{11} = \frac{1 - c_1 - c_2 - c_3}{4}. \quad (C7)$$

In the following one introduces the operations X-control (X) and Hadamard (H) defined as [86]:

$$X = \begin{pmatrix} 1 & 0 & 0 & 0 \\ 0 & 0 & 0 & 1 \\ 0 & 0 & 1 & 0 \\ 0 & 1 & 0 & 0 \end{pmatrix}, \quad H = \frac{1}{\sqrt{2}} \begin{pmatrix} 1 & 1 \\ 1 & -1 \end{pmatrix}. \quad (C8)$$

The *stage II* of the circuit emulates the unitary evolution of the SPE-phonon system. Here, let us consider the evolution of a quantum state $\rho(0)$ under a trace-preserving quantum operation $\rho(t)$ [87],

$$\rho(t) = \sum_{i,j} (E_i \otimes E_j) \rho(0) (E_i \otimes E_j), \quad (C9)$$

where $\{E_k\}$ is the set of Kraus operators associated to a decoherence process of a single qubit [86].

In our case, the dynamics of the qubit is given by the following Kraus operators

$$E_0(t) = \sqrt{\frac{1 + \Theta(t)}{2}} I, \quad E_1(t) = \sqrt{\frac{1 - \Theta(t)}{2}} \sigma^z, \quad (C10)$$

where $\Theta(t) = \sqrt{A}$ defined in Eq. B2.

To finish this stage, one applies the operation controlled-RX gate [86] with the angle $\chi = 2 \arccos[\Theta(t)]$.

The *stage III* is responsible for the SPEs evolution under the effects of quantum noise. For this, we consider the Amplitude damping channel (AD) with the angle θ defined as [88]:

$$\theta = 2 \arccos \left(\sqrt{p_{AD}(t)} \right) \quad (C11)$$

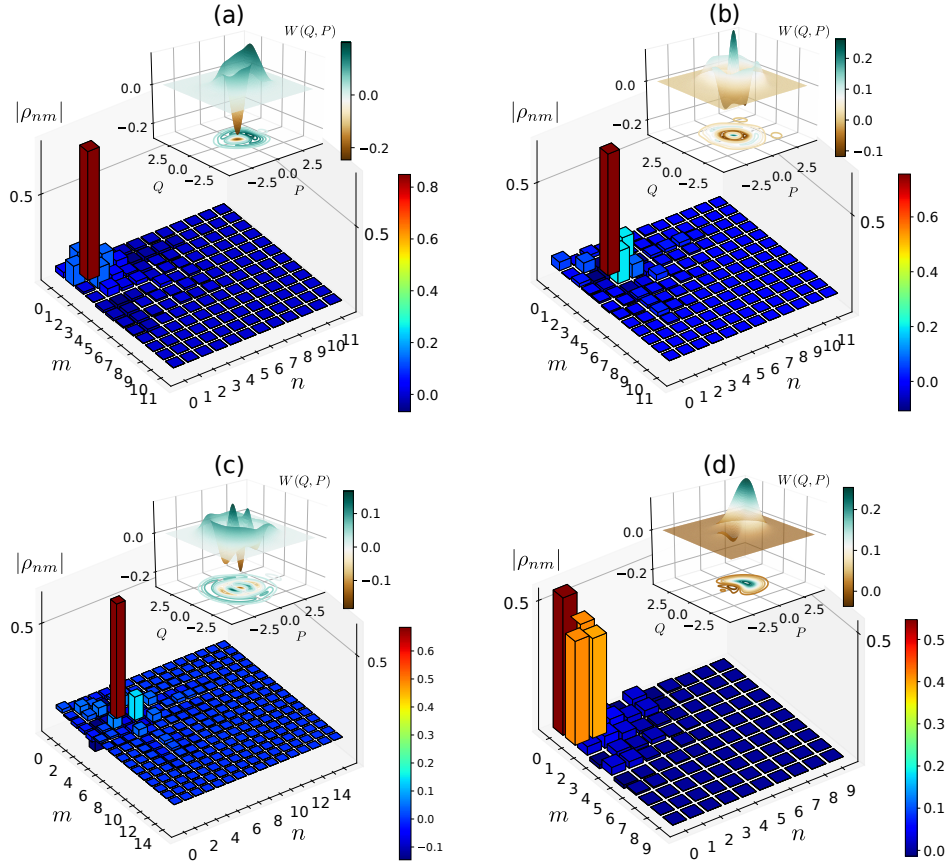


Figure 9. Generation of phonon Fock and qubit states for two equivalent SPEs, i.e. $\Delta_1 = \Delta_2 = \Delta$, $\Omega_1 = \Omega_2 = \Omega$, $\alpha_1 = \alpha_2 = \alpha$, and $g_1 = g_2 = 0.33\omega_m$. (a) Single-phonon state with a fidelity $\mathcal{F}_{|1\rangle} = 0.92$ obtained for $\Delta = 0.33$, $\Omega = 0.71$, and $\alpha = 0.15$. (b) Phonon Fock state $|2\rangle$ with a fidelity $\mathcal{F}_{|2\rangle} = 0.88$ for $\Delta = 0.83$, $\Omega = 0.53$, and $\alpha = 0$; (c) Phonon Fock state $|3\rangle$ with a fidelity $\mathcal{F}_{|1\rangle} = 0.82$ for $\Delta = 1.73$, $\Omega = 1.26$, and $\alpha = 0.46$; (d) Phonon-qubit state with a fidelity $\mathcal{F}_{qubit} = 0.94$ for $\Delta = 0.33$, $\Omega = 0.33$, and $\alpha = 0.96$. (inset: Negative values of Wigner function witnesses a quantum state). Other parameters are the same as in Fig. 2

where $p_{AD}(t)$ is given by

$$p_{AD}(t) = e^{-\gamma_s t} \left[\frac{\gamma_s}{r} \sin \frac{rt}{2} + \cos \frac{rt}{2} \right]^2 \quad (C12)$$

where $r = \sqrt{2\gamma_s - \gamma_s^2}$ and γ_s correspond to the SPEs damping rate as in Eq. 6, and the dephasing is not included here explicitly since it appears as an intrinsic noise of the quantum simulator.

Finally, in *stage IV* the measurement of the SPEs is performed, so we can extract the information from the density operator for SPEs after all the evolution.

Appendix D: Generation of phonon quantum states with two SPEs.

Here we present the preparation protocols for phonon Fock and qubit states for the two SPEs case, alternatively to the one-SPE case already considered in the main text. The results are shown in Fig. 9, where the quantum states are generated only when the SPEs system is driven

by an external field, i.e. $\Omega \neq 0$, similarly to Figs. 2-3. The protocol of two SPEs exhibits high fidelities almost similar to the phonon Fock states as compared to the case of one SPE.

For the system of two and three SPEs, we can reproduce similar effects to those observed for the Fock and Qubit phonon states in the case of one SPE, but for a different set of parameters $\{\Omega, \Delta, \alpha\}$, see Fig. 9 in Appendix D. In particular, we observe that for many SPEs involved in the dynamics, the fidelities for the similar quantum states decreases compared to the case of one SPE. This result is expected, as the total decoherence in the dynamics increases with the number of SPEs and thus affects the purity of the quantum phonon state generation.

In conclusion, by the action of the coherent driving, it is possible to transfer periodically the quantum coherence from the SPEs to the phonon mode via the interaction defined by $\hat{\mathcal{H}}_I$. As a result, the corresponding phonon mode is built up in a quantum Fock state $|n = 1\rangle$, $|n = 2\rangle$, etc. On the other hand, without the external driving,

i.e. $\Omega = 0$, it is impossible to get such quantum states, nevertheless one still observes the periodic formation of

a coherent phonon state when $g_b^{(2)}(0) \rightarrow 1$, see orange curve in Fig. 2a).

[1] A. Barfuss, J. Teissier, E. Neu, A. Nunnenkamp, and P. Maletinsky, Strong mechanical driving of a single electron spin, *Nature Physics* **11**, 820 (2015).

[2] U. Bhattacharya, T. Grass, A. Bachtold, M. Lewenstein, and F. Pistoletti, Phonon-induced pairing in quantum dot quantum simulator, *Nano Letters* **21**, 9661 (2021).

[3] S. J. Whiteley, G. Wolfowicz, C. P. Anderson, A. Bourassa, H. Ma, M. Ye, G. Koolstra, K. J. Satzinger, M. V. Holt, F. J. Heremans, *et al.*, Spin-phonon interactions in silicon carbide addressed by gaussian acoustics, *Nature Physics* **15**, 490 (2019).

[4] C. Errando-Herranz, E. Schöll, R. Picard, M. Laini, S. Gyger, A. W. Elshaari, A. Branny, U. Wennberg, S. Barbat, T. Renaud, M. Sartison, M. Brotons-Gisbert, C. Bonato, B. D. Gerardot, V. Zwiller, and K. D. Jöns, Resonance fluorescence from waveguide-coupled, strain-localized, two-dimensional quantum emitters, *ACS Photonics* **8**, 1069 (2021).

[5] F. Peyskens, C. Chakraborty, M. Muneeb, D. Van Thourhout, and D. Englund, Integration of single photon emitters in 2d layered materials with a silicon nitride photonic chip, *Nature Communications* **10**, 4435 (2019).

[6] Y.-H. Ma, Q.-Z. Ding, and E. Wu, Entanglement of two nitrogen-vacancy ensembles via a nanotube, *Phys. Rev. A* **101**, 022311 (2020).

[7] P.-B. Li, Z.-L. Xiang, P. Rabl, and F. Nori, Hybrid quantum device with nitrogen-vacancy centers in diamond coupled to carbon nanotubes, *Phys. Rev. Lett.* **117**, 015502 (2016).

[8] C.-P. Shen, X.-L. Dong, J.-Q. Chen, Y.-F. Qiao, and P.-B. Li, Strong two-phonon correlations and bound states in the continuum in phononic waveguides with embedded siv centers, *Advanced Quantum Technologies* **4**, 2100074 (2021).

[9] X. Wang, A. Miranowicz, H.-R. Li, and F. Nori, Method for observing robust and tunable phonon blockade in a nanomechanical resonator coupled to a charge qubit, *Phys. Rev. A* **93**, 063861 (2016).

[10] Z.-Y. Li, G.-R. Jin, T.-S. Yin, and A. Chen, Two-phonon blockade in quadratically coupled optomechanical systems, *Photonics* **9** (2022).

[11] X.-Y. Yao, H. Ali, F.-L. Li, and P.-B. Li, Nonreciprocal phonon blockade in a spinning acoustic ring cavity coupled to a two-level system, *Phys. Rev. Appl.* **17**, 054004 (2022).

[12] T. T. Tran, C. Elbadawi, D. Totonjian, C. J. Lobo, G. Grossi, H. Moon, D. R. Englund, M. J. Ford, I. Aharonovich, and M. Toth, Robust multicolor single photon emission from point defects in hexagonal boron nitride, *ACS Nano* **10**, 7331 (2016).

[13] S. Michaelis de Vasconcellos, D. Wigger, U. Wurstbauer, A. W. Holleitner, R. Bratschitsch, and T. Kuhn, Single-phonon emitters in layered van der waals materials, *physica status solidi (b)* **259**, 2100566 (2022).

[14] G. Grossi, H. Moon, B. Lienhard, S. Ali, D. K. Efetov, M. M. Furchi, P. Jarillo-Herrero, M. J. Ford, I. Aharonovich, and D. Englund, Tunable and high-purity room temperature single-photon emission from atomic defects in hexagonal boron nitride, *Nature communications* **8**, 1 (2017).

[15] M. Abdi, M.-J. Hwang, M. Aghtar, and M. B. Plenio, Spin-mechanical scheme with color centers in hexagonal boron nitride membranes, *Phys. Rev. Lett.* **119**, 233602 (2017).

[16] M. Abdi and M. B. Plenio, Quantum effects in a mechanically modulated single-photon emitter, *Phys. Rev. Lett.* **122**, 023602 (2019).

[17] L. J. Martínez, T. Pelini, V. Waselowski, J. R. Maze, B. Gil, G. Cassabois, and V. Jacques, Efficient single photon emission from a high-purity hexagonal boron nitride crystal, *Phys. Rev. B* **94**, 121405 (2016).

[18] D. Wigger, R. Schmidt, O. D. Pozo-Zamudio, J. A. Preuß, P. Tonndorf, R. Schneider, P. Steeger, J. Kern, Y. Khodaei, J. Sperling, S. M. de Vasconcellos, R. Bratschitsch, and T. Kuhn, Phonon-assisted emission and absorption of individual color centers in hexagonal boron nitride, *2D Materials* **6**, 035006 (2019).

[19] J.-W. Jiang, B.-S. Wang, and H. S. Park, Topologically protected interface phonons in two-dimensional nanomaterials: hexagonal boron nitride and silicon carbide, *Nanoscale* **10**, 13913 (2018).

[20] X. Li, C. Xia, Y. Pan, M. Gao, H. Chen, and L. Zhang, Topological chiral phonons along the line defect of intralayer heterojunctions, *Phys. Rev. B* **104**, 054103 (2021).

[21] J.-W. Jiang and H. S. Park, Strain tunable phononic topological bandgaps in two-dimensional hexagonal boron nitride, *Journal of Applied Physics* **125** (2018).

[22] R. Kumar, D. Das, E. Muñoz, and A. K. Singh, Critical sublattice symmetry breaking: A universal criterion for dirac cone splitting, *The Journal of Physical Chemistry C* **123**, 23082 (2019).

[23] D. Das, S. Bhattacharyya, E. Muñoz, and A. K. Singh, Strain-induced chiral symmetry breaking leads to large dirac cone splitting in graphene/graphane heterostructure, *Phys. Rev. B* **94**, 115438 (2016).

[24] L. Ju, Z. Shi, N. Nair, Y. Lv, C. Jin, J. Velasco Jr, C. Ojeda-Aristizabal, H. A. Bechtel, M. C. Martin, A. Zettl, *et al.*, Topological valley transport at bilayer graphene domain walls, *Nature* **520**, 650 (2015).

[25] F. Zhang, J. Jung, G. A. Fiete, Q. Niu, and A. H. MacDonald, Spontaneous quantum hall states in chirally stacked few-layer graphene systems, *Phys. Rev. Lett.* **106**, 156801 (2011).

[26] W. Yao, S. A. Yang, and Q. Niu, Edge states in graphene: From gapped flat-band to gapless chiral modes, *Phys. Rev. Lett.* **102**, 096801 (2009).

[27] J. Jung, F. Zhang, Z. Qiao, and A. H. MacDonald, Valley-hall kink and edge states in multilayer graphene, *Phys. Rev. B* **84**, 075418 (2011).

[28] F. Munoz, H. P. O. Collado, G. Usaj, J. O. Sofo, and C. A. Balseiro, Bilayer graphene under pressure: Electron-hole symmetry breaking, valley hall effect, and

landau levels, Phys. Rev. B **93**, 235443 (2016).

[29] R. Hidalgo-Sacoto, R. I. Gonzalez, E. E. Vogel, S. Alende, J. D. Mella, C. Cardenas, R. E. Troncoso, and F. Munoz, Magnon valley hall effect in cri_3 -based van der waals heterostructures, Phys. Rev. B **101**, 205425 (2020).

[30] R. K. Pal and M. Ruzzene, Edge waves in plates with resonators: an elastic analogue of the quantum valley hall effect, New Journal of Physics **19**, 025001 (2017).

[31] P. Auburger and A. Gali, Towards ab initio identification of paramagnetic substitutional carbon defects in hexagonal boron nitride acting as quantum bits, Phys. Rev. B **104**, 075410 (2021).

[32] N. Mendelson, D. Chugh, J. R. Reimers, T. S. Cheng, A. Gottscholl, H. Long, C. J. Mellor, A. Zettl, V. Dyakonov, P. H. Beton, *et al.*, Identifying carbon as the source of visible single-photon emission from hexagonal boron nitride, Nature materials **20**, 321 (2021).

[33] C. Jara, T. Rauch, S. Botti, M. A. L. Marques, A. Norambuena, R. Coto, J. E. Castellanos-Águila, J. R. Maze, and F. Munoz, First-principles identification of single photon emitters based on carbon clusters in hexagonal boron nitride, The Journal of Physical Chemistry A **125**, 1325 (2021).

[34] F. Pinilla, N. Vasquez, J. R. Maze, C. Cárdenas, and F. Munoz, Carbon-based single photon emitters in hexagonal boron nitride with triplet ground state (2022), arXiv:2209.13735 [cond-mat.mtrl-sci].

[35] K. Li, T. J. Smart, and Y. Ping, Carbon trimer as a 2 ev single-photon emitter candidate in hexagonal boron nitride: A first-principles study, Phys. Rev. Mater. **6**, L042201 (2022).

[36] V. Ivády, G. Barcza, G. Thiering, S. Li, H. Hamdi, J.-P. Chou, Ö. Legeza, and A. Gali, Ab initio theory of the negatively charged boron vacancy qubit in hexagonal boron nitride, npj Computational Materials **6**, 41 (2020).

[37] M. Kianinia, S. White, J. E. Fröch, C. Bradac, and I. Aharonovich, Generation of spin defects in hexagonal boron nitride, ACS Photonics **7**, 2147 (2020).

[38] A. Kopp and K. L. Hur, Universal and measurable entanglement entropy in the spin-boson model, Phys. Rev. Lett. **98**, 220401 (2007).

[39] T. A. Costi and R. H. McKenzie, Entanglement between a qubit and the environment in the spin-boson model, Phys. Rev. A **68**, 034301 (2003).

[40] J. M. Martinis, S. Nam, J. Aumentado, and C. Urbina, Rabi oscillations in a large josephson-junction qubit, Phys. Rev. Lett. **89**, 117901 (2002).

[41] Y. Makhlin, G. Schön, and A. Shnirman, Quantum-state engineering with josephson-junction devices, Rev. Mod. Phys. **73**, 357 (2001).

[42] L. R. Sletten, B. A. Moores, J. J. Viennot, and K. W. Lehnert, Resolving phonon fock states in a multimode cavity with a double-slit qubit, Phys. Rev. X **9**, 021056 (2019).

[43] C. Samanta, S. L. De Bonis, C. B. Møller, R. Tormo-Queralt, W. Yang, C. Urgell, B. Stamenic, B. Thibeault, Y. Jin, D. A. Czaplewski, F. Pistolesi, and A. Bachtold, Nonlinear nanomechanical resonators approaching the quantum ground state, Nature Physics (2023).

[44] A. Bienfait, K. J. Satzinger, Y. Zhong, H.-S. Chang, M.-H. Chou, C. R. Conner, É. Dumur, J. Grebel, G. A. Peairs, R. G. Povey, *et al.*, Phonon-mediated quantum state transfer and remote qubit entanglement, Science **364**, 368 (2019).

[45] G. D. de Moraes Neto, V. Montenegro, V. F. Teizen, and E. Vernek, Dissipative phonon-fock-state production in strong nonlinear optomechanics, Phys. Rev. A **99**, 043836 (2019).

[46] A. Kowalewska-Kudłaszyk, S. I. Abo, G. Chimczak, J. Peřina, F. Nori, and A. Miranowicz, Two-photon blockade and photon-induced tunneling generated by squeezing, Phys. Rev. A **100**, 053857 (2019).

[47] J. Johansson, P. Nation, and F. Nori, Qutip 2: A python framework for the dynamics of open quantum systems, Computer Physics Communications **184**, 1234 (2013).

[48] J. D. Cohen, S. M. Meenehan, G. S. MacCabe, S. Gröblacher, A. H. Safavi-Naeini, F. Marsili, M. D. Shaw, and O. Painter, Phonon counting and intensity interferometry of a nanomechanical resonator, Nature **520**, 522 (2015).

[49] I. Söllner, L. Midolo, and P. Lodahl, Deterministic single-phonon source triggered by a single photon, Phys. Rev. Lett. **116**, 234301 (2016).

[50] A. Osada, K. Taniguchi, M. Shigefuji, and A. Noguchi, Feasibility study on ground-state cooling and single-phonon readout of trapped electrons using hybrid quantum systems, Phys. Rev. Res. **4**, 033245 (2022).

[51] D. Niemietz, P. Farrera, S. Langenfeld, and G. Rempe, Nondestructive detection of photonic qubits, Nature **591**, 570 (2021).

[52] A. P. Reed, K. H. Mayer, J. D. Teufel, L. D. Burkhart, W. Pfaff, M. Reagor, L. Sletten, X. Ma, R. J. Schoelkopf, E. Knill, and K. W. Lehnert, Faithful conversion of propagating quantum information to mechanical motion, Nature Physics **13**, 1163 (2017).

[53] E. A. Wollack, A. Y. Cleland, R. G. Gruenke, Z. Wang, P. Arrangoiz-Arriola, and A. H. Safavi-Naeini, Quantum state preparation and tomography of entangled mechanical resonators, Nature **604**, 463 (2022).

[54] IBM Quantum.

[55] W. K. Wootters, Entanglement of formation of an arbitrary state of two qubits, Phys. Rev. Lett. **80**, 2245 (1998).

[56] R. Horodecki, P. Horodecki, M. Horodecki, and K. Horodecki, Quantum entanglement, Rev. Mod. Phys. **81**, 865 (2009).

[57] C. H. Bennett and D. P. DiVincenzo, Quantum information and computation, nature **404**, 247 (2000).

[58] R. Coto, M. Orszag, and V. Eremeev, Generation and protection of a maximally entangled state between many modes in an optical network with dissipation, Phys. Rev. A **93**, 062302 (2016).

[59] L. Henderson and V. Vedral, Classical, quantum and total correlations, Journal of Physics A: Mathematical and General **34**, 6899 (2001).

[60] H. Ollivier and W. H. Zurek, Quantum discord: A measure of the quantumness of correlations, Phys. Rev. Lett. **88**, 017901 (2001).

[61] S. Luo, Quantum discord for two-qubit systems, Phys. Rev. A **77**, 042303 (2008).

[62] A. Datta, A. Shaji, and C. M. Caves, Quantum discord and the power of one qubit, Phys. Rev. Lett. **100**, 050502 (2008).

[63] B. P. Lanyon, M. Barbieri, M. P. Almeida, and A. G. White, Experimental quantum computing without entanglement, Phys. Rev. Lett. **101**, 200501 (2008).

[64] B. Dakić, Y. O. Lipp, X. Ma, M. Ringbauer, S. Kropatschek, S. Barz, T. Paterek, V. Vedral, A. Zeilinger, Č. Brukner, and P. Walther, Quantum discord as resource for remote state preparation, *Nature Physics* **8**, 666 (2012).

[65] R. Coto, V. Montenegro, V. Eremeev, D. Mundarain, and M. Orszag, The power of a control qubit in weak measurements, *Scientific Reports* **7**, 6351 (2017).

[66] K. Modi, A pedagogical overview of quantum discord, *Open Systems & Information Dynamics* **21**, 1440006 (2014), <https://doi.org/10.1142/S123016121440006X>.

[67] A. Bera, T. Das, D. Sadhukhan, S. S. Roy, A. Sen(De), and U. Sen, Quantum discord and its allies: a review of recent progress, *Reports on Progress in Physics* **81**, 024001 (2017).

[68] M. Ali, A. R. P. Rau, and G. Alber, Quantum discord for two-qubit x states, *Phys. Rev. A* **81**, 042105 (2010).

[69] C. Wang and Q.-H. Chen, Exact dynamics of quantum correlations of two qubits coupled to bosonic baths, *New Journal of Physics* **15**, 103020 (2013).

[70] J. Maziero, L. C. Céleri, R. M. Serra, and V. Vedral, Classical and quantum correlations under decoherence, *Phys. Rev. A* **80**, 044102 (2009).

[71] L. Mazzola, J. Piilo, and S. Maniscalco, Sudden transition between classical and quantum decoherence, *Phys. Rev. Lett.* **104**, 200401 (2010).

[72] J.-S. Xu, X.-Y. Xu, C.-F. Li, C.-J. Zhang, X.-B. Zou, and G.-C. Guo, Experimental investigation of classical and quantum correlations under decoherence, *Nature Communications* **1**, 7 (2010).

[73] V. Eremeev, N. Ciobanu, and M. Orszag, Thermal effects on sudden changes and freezing of correlations between remote atoms in a cavity quantum electrodynamics network, *Opt. Lett.* **39**, 2668 (2014).

[74] G. Kresse and J. Hafner, Ab initio molecular dynamics for liquid metals, *Phys. Rev. B* **47**, 558 (1993).

[75] G. Kresse and J. Hafner, Ab initio molecular-dynamics simulation of the liquid-metal–amorphous-semiconductor transition in germanium, *Phys. Rev. B* **49**, 14251 (1994).

[76] G. Kresse and J. Furthmüller, Efficiency of ab-initio total energy calculations for metals and semiconductors using a plane-wave basis set, *Comput. Mater. Sci.* **6**, 15 (1996).

[77] G. Kresse and D. Joubert, From ultrasoft pseudopotentials to the projector augmented-wave method, *Phys. Rev. B* **59**, 1758 (1999).

[78] J. P. Perdew, K. Burke, and M. Ernzerhof, Generalized gradient approximation made simple, *Phys. Rev. Lett.* **77**, 3865 (1996).

[79] U. Herath, P. Tavadze, X. He, E. Bousquet, S. Singh, F. Muñoz, and A. H. Romero, Pyprocar: A python library for electronic structure pre/post-processing, *Computer Physics Communications* **251**, 107080 (2020).

[80] A. Togo, L. Chaput, T. Tadano, and I. Tanaka, Implementation strategies in phonopy and phono3py, *J. Phys. Condens. Matter* **35**, 353001 (2023).

[81] A. Alkauskas, B. B. Buckley, D. D. Awschalom, and C. G. V. de Walle, First-principles theory of the luminescence lineshape for the triplet transition in diamond nv centres, *New Journal of Physics* **16**, 073026 (2014).

[82] B. Hourahine, B. Aradi, V. Blum, F. Bonafé, A. Buccheri, C. Camacho, C. Cevallos, M. Deshaye, T. Dumitriță, A. Dominguez, *et al.*, Dftb+, a software package for efficient approximate density functional theory based atomistic simulations, *The Journal of chemical physics* **152**, 124101 (2020).

[83] M. Elstner, D. Porezag, G. Jungnickel, J. Elsner, M. Haugk, T. Frauenheim, S. Suhai, and G. Seifert, Self-consistent-charge density-functional tight-binding method for simulations of complex materials properties, *Phys. Rev. B* **58**, 7260 (1998).

[84] M. B. Pozzobom and J. Maziero, Preparing tunable bell-diagonal states on a quantum computer, *Quantum Information Processing* **18** (2019).

[85] E. Riedel Gårding, N. Schwaller, C. L. Chan, S. Y. Chang, S. Bosch, F. Gessler, W. R. Laborde, J. N. Hernandez, X. Si, M.-A. Dupertuis, and N. Macris, Bell diagonal and werner state generation: Entanglement, non-locality, steering and discord on the ibm quantum computer, *Entropy* **23** (2021).

[86] M. A. Nielsen and I. L. Chuang, *Quantum Computation and Quantum Information* (Cambridge University Press, 2010).

[87] W. Yao-Kun, F. Shao-Ming, and W. Zhi-Xi, Dynamics of quantum coherence in bell-diagonal states under markovian channels*, *Communications in Theoretical Physics* **71** (2019).

[88] G. García-Pérez, Rossi, M. A. C., and S. Maniscalco, Ibm q experience as a versatile experimental testbed for simulating open quantum systems, *npj Quantum Information* **6** (2020).